Cellulose (2022) 29:8229–8242
https://doi.org/10.1007/s10570-022-04765-6

ORIGINAL RESEARCH

Efficient preparation of holocellulose nanofibers and their reinforcement potential

Qiqi Ding · Jun Rao · Ziwen Lv · Xue Gong · Baozhong Lü · Ying Guan · Junli Ren · Feng Peng

Received: 6 April 2022 / Accepted: 14 July 2022 / Published online: 1 August 2022

Abstract Preparation of cellulose nanofibers or nanocrystals with large-scale by traditional methods is facing a scientific challenge due to the complex technological process, excessive energy consumption and environmental pollution. Herein, the novel holocellulose nanofibers (HNFs) were obtained from different lignocellulosic biomass, including wheat straw, bamboo (*Neosinocalamus affinis)*, hardwood (*Populus nigra*), and softwood (*Monterey pine*) by mechanical or TEMPO-mediated oxidation method. Compared with TEMPO-mediated oxidation, HNFs prepared by mechanical method exhibit higher hemicellulose content, well preserved natural structure (a core-shell structure), and high crystallinity. Significantly, the mechanical processing is simple and more suitable for large-scale production. After introducing HNFs, the mechanical property of polyvinyl alcohol (PVA) film increased dramatically. In particular, the Young's modulus of HNFs/PVA composite film is 25.12 times higher than that of pure PVA. These results suggest that HNFs can be used as versatile reinforcement to construct composite materials with excellent performance.

Graphical abstract A novel nano-holocellulose could be replace cellulose to constructfunctional material was prepared by mechanical or TEMPO-mediated oxidation methods from different lignocellulosic biomass.

Supplementary Information The online version contains supplementary material available at https://doi.org/10.1007/s10570-022-04765-6.

Q. Ding · J. Rao (✉) · Z. Lv · X. Gong · B. Lü · F. Peng
Beijing Key Laboratory of Lignocellulosic Chemistry, Beijing Forestry University, Beijing 100083, China
e-mail: rjsweetheart@outlook.com

Y. Guan
Forestry and Landscape Architecture, Anhui Agricultural University, Hefei 230036, China

J. Ren
State Key Laboratory of Pulp and Paper Engineering, South China University of Technology, Guangzhou 510640, China

F. Peng (✉)
MOE Engineering Research Center of Forestry Biomass Materials and Bioenergy, Beijing Forestry University, Beijing 100083, China
e-mail: fengpeng@bjfu.edu.cn

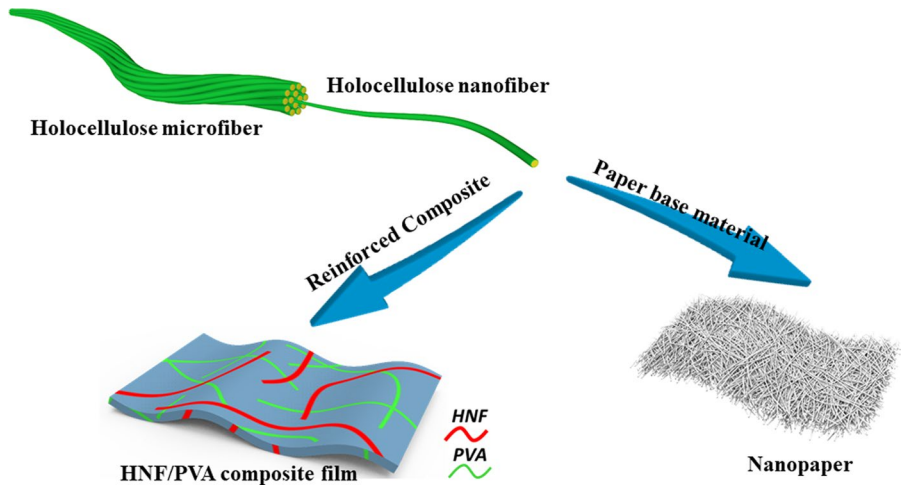

Keywords Holocellulose nanofibers · Mechanical method · TEMPO oxidation · Nanopaper · Mechanical property

Introduction

The increasing production and excessive use of plastic materials will inevitably accumulate non-biodegradable waste in the natural environment, causing serious environmental pollution and public health issues (MacLeod et al. 2021; Santos et al. 2021). The plastic pollution will become poorly reversible once it evolves into micro- and nano-plastic particles caused by degradation weathering process. These plastic particles can accumulate in the human body through the food chain, threatening human health. Therefore, it is highly desired to develop the degradable bio-based plastics derived from wood, crop straw, shellfish, or other bio-based feedstocks to replace conventional petroleum-based plastics (Altman 2021).

As the most abundant biomacromolecule on earth, cellulose is composed of linear chains containing the monomer D-glucose linked with β-(1–4) glycosidic bonds (Klemm et al. 2005). It is an almost inexhaustible polymeric raw material that can be obtained from diverse sources by pulping, including crop straw (e.g., cotton stalk, wheat straw, bagasse), wood, bamboo, and other green plants. The application of cellulose has been widely expanded with the discovery of nanocellulose (cellulose nanofiber and nanocrystal). The hierarchical structure of nanocellulose endows its fascinating properties, such as excellent mechanical property, low coefficient of thermal expansion, and high surface functionality (Klemm et al. 2005; Kontturi et al. 2006). Nanocellulose can be assembled into surfactants, bio-membranes, flexible paper, and robust hydrogels, which have a great potential for Pickering emulsion (Alila et al. 2005; Bahsi Kaya et al. 2022), high-performance materials (Jia et al. 2019; Li et al. 2019), flexible transparent substrates for electronics or sensors (Wang et al. 2021; Zhu et al. 2016), and multifunctional biological hydrogels (Hausmann et al. 2020; Isobe et al. 2013).

The preparation methods of nanocellulose include sulfuric acid hydrolysis (Habibi et al. 2010), oxidation (Isogai et al. 2011; Liu et al. 2020), etherification (Wang et al. 2020), esterification (Chen et al. 2016), and mechanical treatment (Abdul Khalil et al. 2014; Zhang et al. 2015). Among these chemical methods, 2,2,6,6-tetramethylpiperidinyl-1-oxyl oxidation (known as TEMPO-mediated oxidation method) has been widely investigated, because it can resolve the excessive energy consumption and render cellulose nanofiber has a high surface charge. The high electric density on the surface of cellulose nanofiber is produced by carboxylate groups formed on the C6 position of monosaccharide units, resulting in high colloidal stability (Alves et al. 2020; Isogai et al. 2011; Saito et al. 2007). However, TEMPO-mediated oxidation method has some drawbacks for large-scale manufacturing, such as the TEMPO catalyst is expensive and toxic and the

production period is long. Furthermore, the structure of cellulose could be destroyed during the oxidation process, which potentially triggers degradation and causes performance degradation (Fukuzumi et al. 2010). To overcome these drawbacks and realize efficient preparation of nanocellulose in high yield, mechanical treatments, including high pressure homogenization (Nakagaito and Yano 2004), micro-fluidization (Ferrer et al. 2012), grinding (Wang et al. 2012), and high intensity ultrasonication (Wang and Cheng 2009), serve as alternatives to isolate cellulose nanofiber from lignocellulose. Energy consumption is the main drawback in mechanical isolation processes. The raw material needs to be pretreated with enzyme, alkaline-acid, or ionic liquids to destroy the hydrogen bond network caused by hydroxy groups (Abdul Khalil et al. 2014; Liu et al. 2019). Therefore, it is still a considerable challenge to prepare nanocellulose by mechanical methods, which can avoid the need for tedious pretreatment processes.

Herein, we developed a novel pretreatment-free mechanical method (grinding) to prepare holocellulose nanofibers. In order to verify the universality of this method, four different lignocellulosic resources, wheat straw, bamboo (*Neosinocalamus affinis)*, hardwood (*Populus nigra*), and softwood (*Monterey pine*) were selected to prepare HNFs. Meanwhile, TEMPO-mediated oxidation method was also applied to prepare HNFs. HNFs obtained by mechanical method showed a high hemicellulose content, well-preserved natural structure (a core-shell structure), and high crystallinity. The corresponding nanopaper exhibited more superior mechanical properties than those obtained by the TEMPO-mediated oxidation method. Meanwhile, the HNFs were employed as reinforcement introduced into polymer matrix to construct high-performance materials. The mechanical properties of PVA film have been dramatically increased by incorporating HNFs, suggesting HNFs can be used as versatile reinforcement to construct composite materials with high performance.

Materials and methods

Materials

The hardwood (*Populus nigra*), softwood (*Monterey pine*), and bamboo (*Neosinocalamus affinis*) were purchased from the local market. Wheat straw was obtained from our previous work (Rao et al. 2021). Sodium chlorite (80%), sodium bromide (99%), acetic acid (99.5%), sodium hypochlorite, 2,2,6,6-tetramethylpiperidin-1-oxygen-radical (98%), and polyvinyl alcohol (PVA, $Mw = \sim 67\ 000$ g/mol) were purchased from Macklin Inc (China). All reagents used in this study were of analytical grade and used without any purification. The holocellulose was prepared by delignification using a mixed aqueous solution of acetic acid and sodium chlorite according to our previous work (Peng et al. 2012).

Preparation of HNFs from different lignocellulosic biomass

HNFs prepared by mechanical method (MNF). Preparation of HNFs by mechanical method was based on our previous work (Rao et al. 2021). The typical preparation process was as follows: the holocellulose was dispersed in deionized water (1%) for 2 d to ensure fiber swelling. Then, the mixture was injected into the ultrafine grinder (MKCA6-5JM, MASUKO) for mechanical defibrillation, and the HNFs were prepared by adjusting the refiner plates spacing and the grinding time. Here, the space between the refiner plate and the grinding time was set as ~1 μm and 4 h, respectively. The HNFs prepared by mechanical method from wheat straw, bamboo, hardwood, and softwood were marked as MNF-S, MNF-B, MNF-P, and MNF-MP, respectively.

HNFs prepared by TEMPO method (TONF). The TEMPO-mediated oxidation of holocellulose was executed according to our previous work with modifications (Rao et al. 2021). Briefly, holocellulose (2 g) was suspended in water (150 mL) containing TEMPO (0.04 g) and sodium bromide (0.2 g). The mixture was stirred at ambient temperature for 30 min, followed by adding aqueous NaClO (7%, 21.27 mL; 10 mmol/g, NaClO/holocellulose) under stirring. The pH of the reaction system was maintained at 10 ± 0.2 by continuously adding 0.5 M NaOH. The reaction was terminated after 12 h by adding 0.5 M HCl to adjust the pH to 7. In order to remove the unreacted reagents and metal salt, the oxidized holocellulose was then purified by dialysis for a week. After that, the holocellulose fibers were mechanically treated in a high-pressure homogenizer (AH-NANO, China) at 800 psi for 10 passes to obtain a stabilized and homogeneous HNFs suspension. The HNFs prepared by TEMPO method from wheat straw, bamboo, hardwood, and

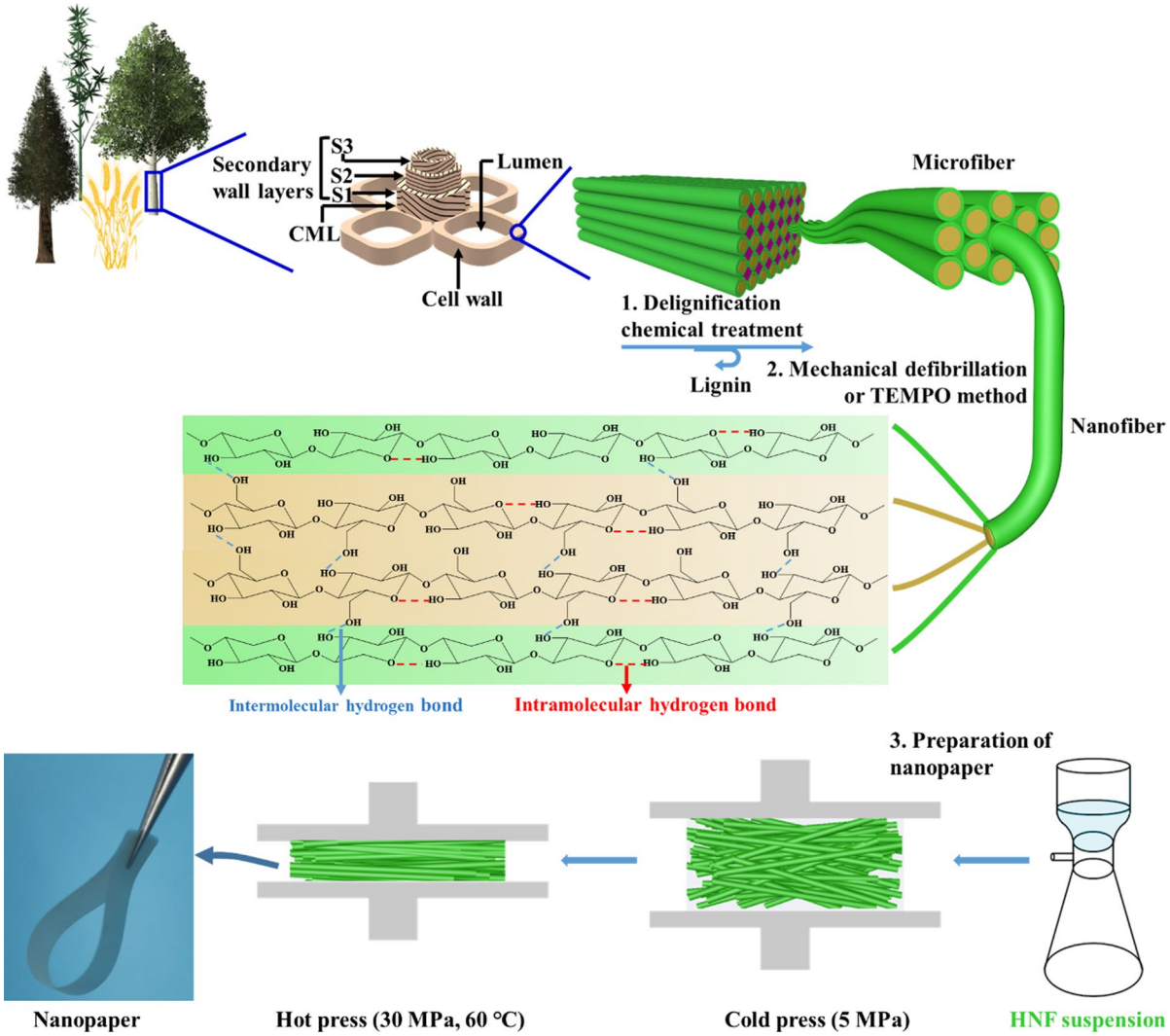

Fig. 1 Schematic representation of the processing route from various plants to HNFs (a central cellulose core with a hemicellulose coating) and their corresponding strong and tough nanopaper prepared by vacuum filtration and compression process

softwood were named as TEMPO-S, TEMPO-B, TEMPO-P, and TEMPO-MP, respectively.

Preparation of holocellulose-based nanopaper

Holocellulose-based nanopaper was fabricated by a vacuum filtration-hot compression process, as presented in Fig. 1. The HNFs suspension (0.2 wt%, 20 mL) was vacuum filtered on a cellulose acetate membrane (pore diameter, 0.45 μm; diameter, 47 mm). The wet nanopaper was then placed between two metal plates and pressed under a load of 5 MPa for 4 h, followed by hot-pressing under a load of 30 MPa at 60 °C for 10 h. After that, the nanopaper was carefully peeled from the filter membrane to obtain free-standing nanopaper.

Preparation of HNFs/PVA films

The HNFs/PVA composite films were prepared by solution-casting. PVA was dissolved in water at 60 °C for 1 h under magnetic stirring to obtain a clear solution with a concentration of 20 mg/mL.

The TEMPO-B and MHF-B was then added into the PVA solution (2% based on PVA), respectively, followed by stirring under ambient temperature for 24 h to form a homogeneous solution. The HNFs/PVA homogeneous solution was casted into a culture dish of polystyrene and dried under ambient temperature for 7 d. Finally, the composite films were peeled off from the culture dish carefully. As a reference, neat PVA film was prepared using the same procedure.

Characterization methods

The compositions of the samples were evaluated by NREL standard protocol (Sluiter et al. 2008). Fourier transform infrared (FT-IR) spectra of the samples were recorded on a Bruker Tensor II equipment at the wavenumber range of 4000–500 cm^{-1}. The wide-angle X-ray diffraction (XRD) patterns of the samples were measured by X-ray diffractometer (Bruker D8) at 40 kV and 40 mA, the 2θ range of 5–60° with a speed of $2°{\cdot}min^{-1}$. The Crystallinity index (*CrI*) was calculated from the intensity of the 200 peak (I_{200}, $2\theta = 22.6°$) and the intensity minimum between the peaks at 200 and 110 (I_{am}, $2\theta = 18.7°$) by using the empirical equation as below:

$$CrI = \frac{I_{200} - I_{am}}{I_{200}} * 100$$

The zeta potential of the samples was determined by Zetasizer Nano Z (Malvern, United Kingdom). The morphology and size of the nanofibers were investigated by atomic force microscope (Bruker Dimension Icon). The suspension liquid of the samples was dropped on the mica sheet, then dried at room temperature before observed. The scan mode and area were ScanAsyst Mode and 5 × 5 μm, respectively. The length and diameter distribution of samples were measured by Image J software. Thermogravimetric analysis of the samples was performed using DTG-60 (Shimadzu, Japan). The morphologies of the nanopaper and composite films (HNFs/PVA) were investigated by the scanning electron microscope (Hitachi, SU-8010) instrument at 3 kV. Prior to SEM observation, the nanopaper and HNFs/PVA composite films were brittle fractured in liquid nitrogen and then sputter-coated with a thin layer of gold. The mechanical properties of the nanopaper and HNFs/PVA composite films were determined by universal mechanical testing machine with a load cell of 1 kN (Instron 5982). The dimensions of the sample were recorded by vernier caliper and micrometer before measured. At least five repeated measurements of each nanopaper were tested with a strain rate of 2 mm min^{-1} and the average value was used to determine mechanical properties.

Results and discussion

Characteristics of holocellulose nanofibers

Changes in chemical composition (cellulose, hemicellulose, and lignin) and crystallinity of holocellulose and HNFs are summarized in Table 1. Compared

Table 1 Crystallinity index (C_I) and chemical composition of holocelluose and holocellulose nanofibers

Sample	C_I (%)	Lignin (%)	Cellulose (%)	Hemicellulose (%)
Holo-S	61.50	6.78 ± 0.17	39.29 ± 1.03	24.25 ± 1.44
MNF-S	66.28	6.02 ± 0.26	37.29 ± 1.22	20.58 ± 0.37
TEMPO-S	56.93	1.63 ± 0.21	36.00 ± 0.95	10.89 ± 0.31
Holo-B	59.38	1.83 ± 0.30	39.45 ± 0.24	25.92 ± 0.55
MNF-B	61.35	1.41 ± 0.14	38.85 ± 0.32	24.52 ± 0.37
TEMPO-B	57.30	1.13 ± 0.08	33.89 ± 0.56	14.29 ± 1.06
Holo-P	72.01	4.65 ± 0.10	45.45 ± 1.07	20.81 ± 0.78
MNF-P	75.63	4.43 ± 0.08	43.66 ± 2.00	19.61 ± 0.51
TEMPO-P	52.96	1.85 ± 0.14	36.04 ± 1.98	12.25 ± 1.01
Holo-MP	65.07	6.53 ± 0.18	40.66 ± 3.85	22.56 ± 2.82
MNF-MP	68.89	6.18 ± 0.18	37.62 ± 0.96	20.56 ± 0.74
TEMPO-MP	56.90	2.05 ± 0.25	34.52 ± 3.30	14.36 ± 3.31

with holocellulose, hemicellulose dramatically decreased (~10%) in TONF, which was attributed to the efficient removal of hemicellulose under alkaline environment (Chaker et al. 2013). The remaining hemicellulose is mainly xylan without side chain, which exhibits a twofold helical screw ribbon to bind with cellulose through strong hydrogen bond, and cannot be easily isolated under mild alkaline conditions (Gao et al. 2020; Simmons et al. 2016). Meanwhile, the cellulose content significantly decreased, especially in *Populus nigra*, by about 9%, which indicated that the amorphous region was partially degraded due to the destruction of alkaline hydrolysis, which is similar to previous works (Zhao et al. 2017; Saito et al. 2005). In terms of MNF, there was little change in hemicellulose and cellulose content, suggesting that the natural structure (core-shell structure) was well-preserved.

The chemical structures of holocellulose and HNFs were investigated by FT-IR. FT-IR spectra of holocellulose and HNFs are shown in Fig. S1. All the samples exhibit a strong and broad absorption peak ranged from 3200 to 3600 cm^{-1} related to O–H stretching vibration, which are mainly originated from the cellulose and hemicellulose molecules; the characteristic peak at 896 cm^{-1} is attributed to β-(1→4) glycosidic linkages. The peaks ranged from 2800 to 3000 cm^{-1} are assigned to the C–H symmetrical stretching. The peak at 1736 cm^{-1} is corresponded to C=O stretching, originating from the glucuronic acid and acetyl in hemicellulose (Khawas and Deka 2016; Peng et al. 2009; Timell 1967). The peak at 1630 cm^{-1} is assigned to the O–H bending vibration of the absorbed water (Jiang and Hsieh 2013). Compared with holocellulose, the intensity of the peaks belonging to O–H and –C=O vibration remarkably increased in MNF, due to the exposure of abundant hydroxyl and glucuronic acid groups on the surface of the individual nanofibers, resulting in the negative zeta potential ranging from −24.28 to −17.58 mV (Fig. S3). In contrast, the intensity of the peak at 1736 cm^{-1} (–C=O vibration) significantly decreased in HNFs prepared by TEMPO-mediated oxidation method, suggesting that abundant of hemicellulose was removed (Chaker et al. 2013). The new absorption peaks ranged from 1611 to 1620 cm^{-1} were the asymmetric stretching vibration of –COO, indicating that the carboxyl groups were introduced into the molecular chain by TEMPO oxidation (Zhao et al. 2017), resulting in a higher zeta potential ranging from −66.26 to −52.00 mV (Fig. S3).

The crystalline structures of holocellulose and HNFs were further demonstrated in the corresponding XRD patterns (Fig. S2). All samples present similar diffraction patterns, and the peaks for their crystal planes are located at shifted 2θ angles of around 15.2–16.0° (110), 22.0–22.4° (200), and 30.6–35.0° (004), respectively, relating to the presence of different hemicellulose content. These results suggested that the cellulose I_β crystalline structure was maintained after mechanical or TEMPO-oxidation treatment (Liu et al. 2021; Yang et al. 2020). Compared with holocellulose, the crystallinity of MNF is slightly increased, which could be attributed to the removal of amorphous hemicellulose (Yang et al. 2019). Additionally, a highest C_I is observed for holocellulose nanofiber of *Populus nigra* was obtained by mechanical method at 75.63%, which may be due to their natively highly ordered crystalline structure. On the contrary, the crystallinity of HNFs derived from TEMPO-mediated oxidation method decreased significantly, which might result from the degradation of hemicellulose and cellulose under alkaline conditions, consistent with previous works (Saito et al. 2005; Yang et al. 2020). These results show that the native crystalline cellulose structure of mechanical prepared HNFs could be well preserved.

To understand the dimension scale of the prepared holocellulose nanofibers, atomic force microscope (AFM) observations were carried out to visualize the morphology of the HNF. As shown in Figs. 2 and S4, all the samples show clear nanofibrillar structures irrespective of the holocellulose source and the differences in chemical composition. The diameter of HNF obtained from TEMPO-mediated oxidation method is smaller than mechanical method, which could be ascribed to the removal of hemicellulose on the surface of cellulose. Compared with cellulose nanofibers reported in previous literature or TEMPO-mediated oxidation method, the MNF exhibits exceptionally long length ranging from 1860 to 2200 nm, because of the hemicellulose and cellulose were partially degraded in alkaline environment, consistent with the results of crystallinity and component analysis. These results demonstrate that the natural structure of holocellulose could be well-preserved during the mechanical treatment (Van Hai et al. 2018; Yang et al. 2020; Zhu et al. 2017). The structure of holocellulose was

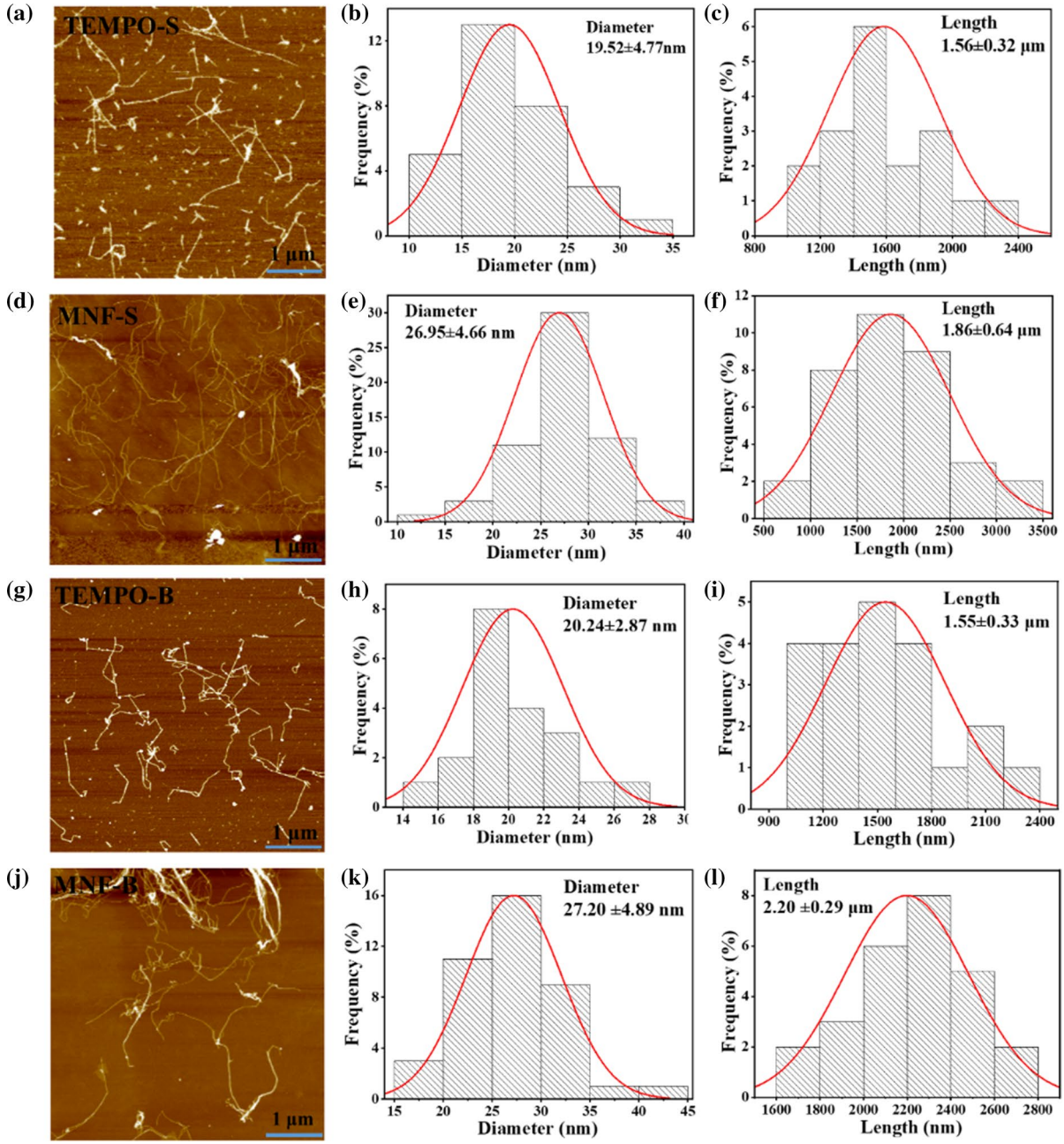

Fig. 2 **a** AFM image of TEMPO-S (scale bar is 1 μm). Diameter (**b**) and length (**c**) distribution of TMPO-S obtained from AFM height profile; TEMPO-S with a 19.52 nm and 1.56 μm length (**d**) AFM image of MNF-S (scale bar is 1 μm). Diameter (**e**) and length (**f**) distribution of MNF-S obtained from AFM height profile; MNF-S with a 26.95 nm diameter and 1.86 μm length. **g** AFM image of TEMPO-B (scale bar is 1 μm). Diameter (**h**) and length (**i**) distribution of TEMPO-B obtained from AFM height profile; TEMPO-B with a 20.24 nm diameter and 1.55 μm length. **j** AFM image of MNF-B (scale bar is 1 μm). Diameter (**k**) and length (**l**) distribution of MNF-B obtained from AFM height profile; MNF-B with a 27.20 nm diameter and 2.20 μm length

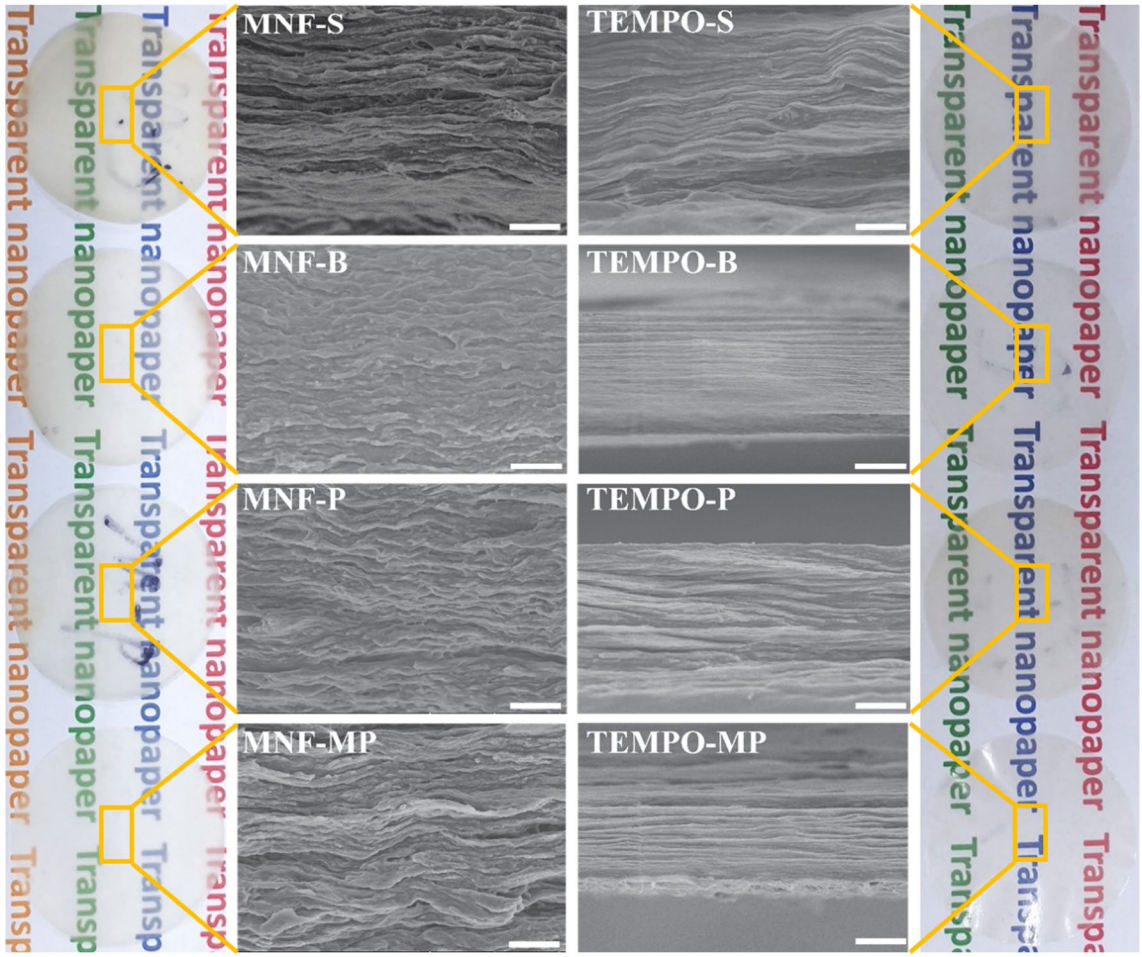

Fig. 3 Photograph and an in-plane layered structure was observed in the cross-section images of the holocellulose-based nanopaper (scale bar is 2 μm)

destroyed after chemical treatment, resulting in a shorter length of nanofiber.

Characteristics of HNFs based nanopaper

The holocellulose-based nanopaper exhibits a high level of optical transmittance exceeding 70% in the visible light region, as shown in Figs. 3 and S5. The diameter of HNFs is less than 30 nm, and the nanofibers and voids between them are much smaller than the wavelength of the visible light, making the nanopaper transparent (Kang et al. 2017). The morphology of holocellulose-based nanopaper was studied by SEM (Fig. 3). All the nanopaper exhibit a densely packed and multilayer structures caused by vacuum-assisted assembly.

Mechanical properties are important for many practical applications of films and papers. The mechanical properties of HNFs based nanopaper were measured by a universal mechanical testing instrument and the characteristic tensile strain-strength curves of different nanopaper are presented in Fig. 4a. The nanopaper prepared from MNF exhibits higher tensile strength, tensile strain, and toughness than those of TEMPO-mediated oxidation method, because the natural structure of holocellulose can be retained. However, the Young's modulus of the nanopaper based on HNFs prepared by TEMPO method is higher. The reason is that the hemicellulose is removed after TEMPO-mediated oxidation, resulting in a stiffer structure of the HNF (Arola et al. 2013; Oksanen et al. 1997). Hence, hemicellulose plays a

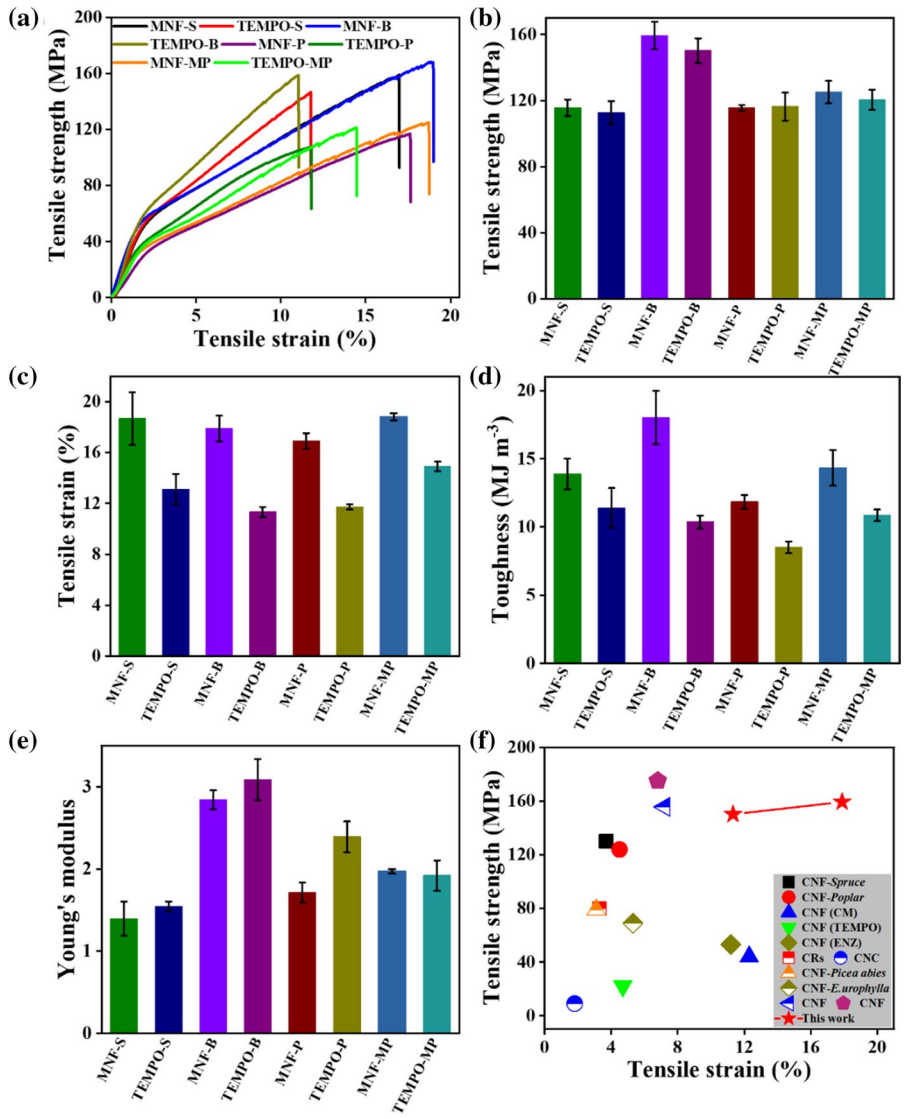

Fig. 4 **a** Typical tensile strength-strain curves of nanopaper. **b** Tensile strength; **c** tensile strain; **d** toughness; **e** Young's modulus of the holocellulose-based nanopaper. **f** Comparison of mechanical properties of holocellulose-based nanopaper and other cellulose-based composites reported in the previous literature (Table S1)

key role in the mechanical properties of nanopaper. The hemicellulose is strongly attached to the cellulose surface as a shell coating and serve as a polymer matrix phase and bonding agent, providing improved stress transfer between HNF and allowing movement of the nanofiber under tensile stress (Galland et al. 2015). Particularly, the nanopaper based on MNF-B exhibits superior comprehensive mechanical properties, the tensile strength, tensile strain, and toughness are 159.39 MPa, 17.89%, and 18.02 MJ m^{-3}, respectively. The possible reason of this result is that the MNF-B has the maximum aspect ratio, leading to an increased binding force between nanofibers, which agrees well with previously reported results (Zhao et al. 2017).

The mechanical properties of the presented holocellulose nanopaper are significantly higher than previous reported cellulose-based nanopaper as shown in Fig. 4f and Table S1 (Chen et al. 2017; Kim et al. 2021; Liu et al. 2017, 2021; Wang et al. 2019; Wei et al. 2021; Zhao et al. 2017). The presented holocellulose nanofiber has fewer defects than typical cellulose nanofiber prepared by TEMPO-mediated oxidation, which will lead to a higher intrinsic nanofiber modulus. More importantly, the natural core-shell structure of HNF prepared from mechanical method is retained. Thus, this work has developed a new route

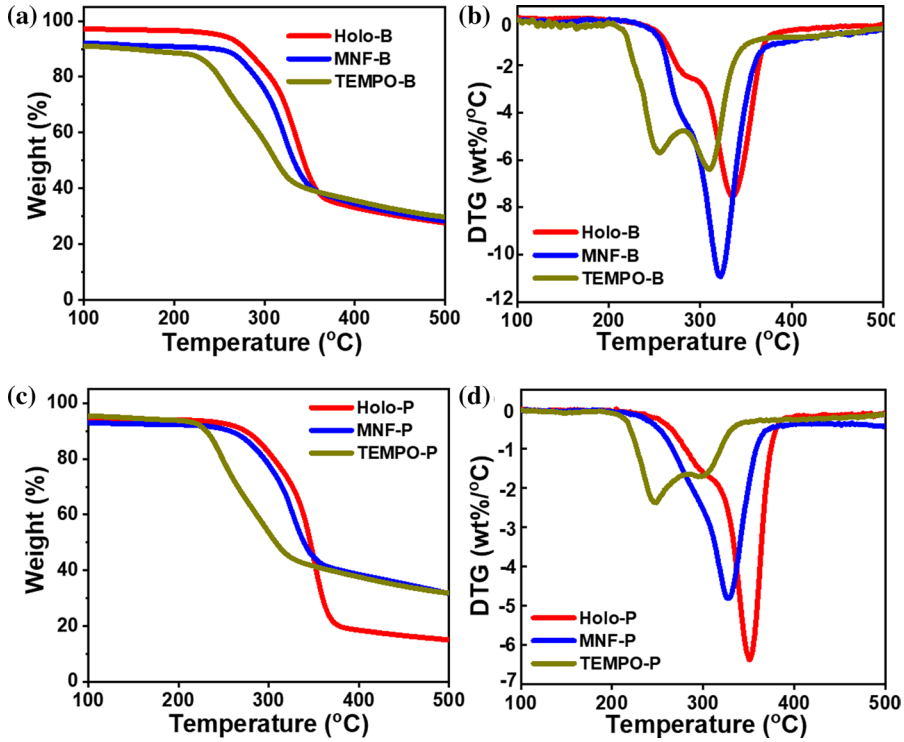

Fig. 5 Thermal stability of the holocellulose and holocellulose-based nanopaper

to prepare HNF which can replace traditional cellulose nanofiber and exhibits a great potential application in the preparation of paper-based materials.

High thermal-stability is required for the practical applications of nanopaper. The thermal-stability of holocellulose and holocellulose-based nanopaper was measured by a thermal gravimetric analyzer, as shown in Figs. 5, S6, and Table S2. For holocellulose and MNF-based nanopaper, there are two degradation stages in the corresponding TG curves, which are caused by the different degradation of hemicellulose (~ 268 °C) and cellulose (~ 355 °C) (Yang et al. 2007). However, the T_2 (the maximum weight loss temperatures) of MNF-based nanopaper is lower than pristine holocellulose, because there is a plentiful exposure of hydroxyl groups, which will be preferentially pyrolysed after mechanical defibrillation. As for TONF-based nanopaper, the DTG curves become broad, and the distinct degradation peaks at approximately 250 °C and 300 °C are observed, which can be assigned to the sodium carboxylate groups and the original cellulose, respectively (Nascimento et al. 2019). Notably, the thermal-stability of TONF-based nanopaper decreased with the increasing degree of oxidation (that is the value of Zeta potential as shown in Fig. S3), suggesting that the decrease in crystallinity of holocellulose (Fukuzumi et al. 2010). These results are in good agreement with the chemical composition and crystallinity analysis.

Characteristics of HNFs/PVA films

It is widely accepted that cellulose nanofibers or nanocrystals are used as reinforcement to fabricate multifunctional composite materials with high performance. To elucidate this concept, HNFs were used as reinforcement to improve the performance of PVA polymer matrix. The transparent nanocomposite films were prepared by solution-casting of the HNFs and PVA mixed solution (Fig. 6a, b). The morphology and mechanical properties of the composite films are measured and presented in Fig. 6c–h. It can be obviously seen that the pure PVA exhibited dense and smooth cross-section (Fig. 6c), which was consistent with previous works (Niu et al. 2018). For the HNFs/PVA composite films, the cross-sections became rougher than that of pure PVA film (Fig. 6d, e). However, the holocellulose nanofibers (white dots) were dispersed uniformly in the matrix without any agglomerations, resulting in a high level

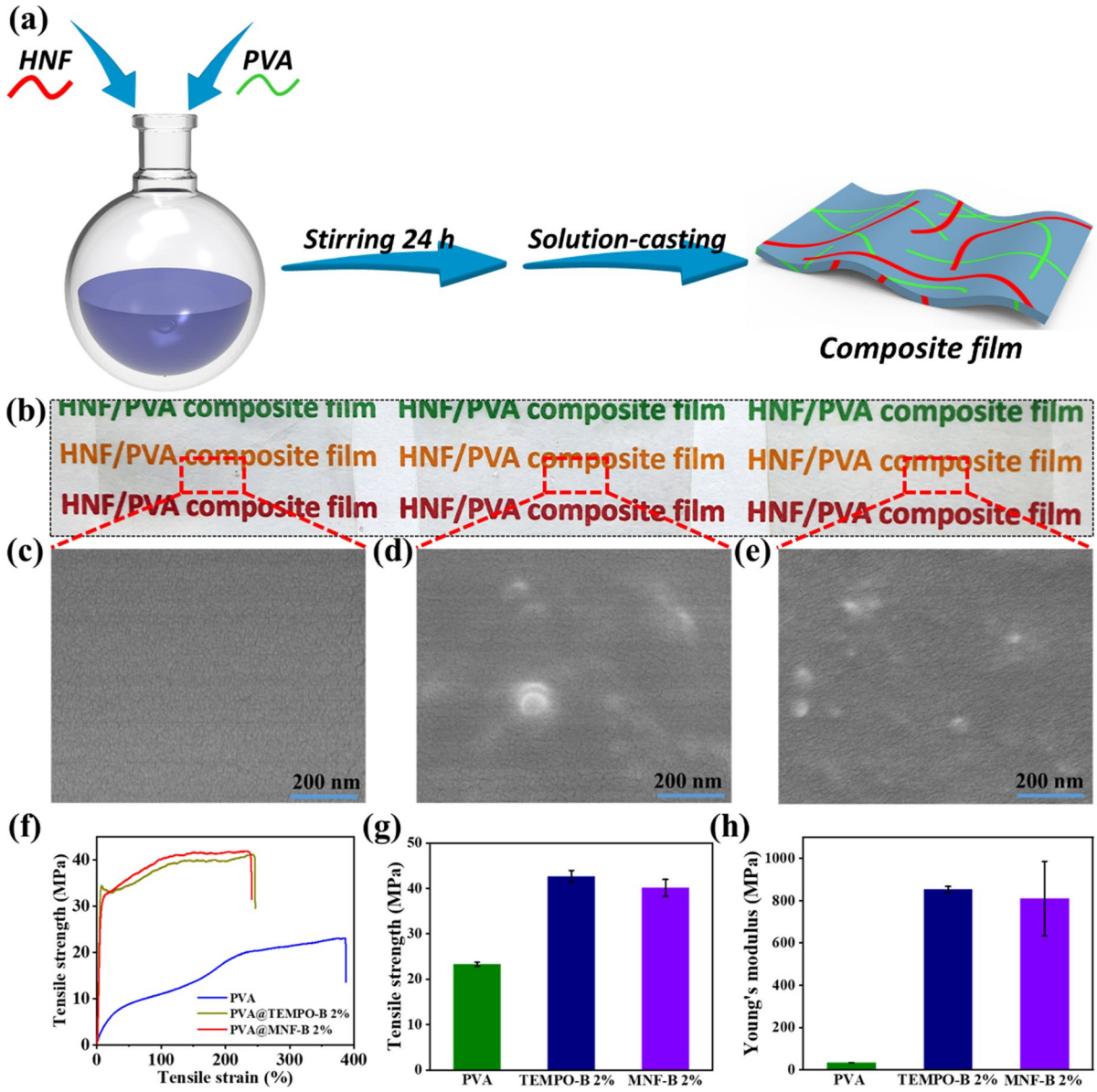

Fig. 6 **a** Schematic representation of the processing route of HNFs/PVA composite film. **b** Photograph of PVA and HNFs/PVA composite films. **c** Cross-section SEM images of PVA; **d** PVA@MNF-B 2%; **e** PVA@TEMPO-B 2%. **f** Typical tensile strength-strain curves of PVA@bamboo HNFs. **g** Tensile strength; **h** Young's modulus of the PVA/Bamboo HNFs composite films

of compatibility as well as interaction between the HNFs and PVA matrix.

In this work, the mechanical properties of HNFs/PVA composite films were measured under ambient conditions (temperature and relative humidity of environment is about 20 °C and 50%). The samples were stored in a temperature humidity chamber (30 °C, RH 60%) before measuring. From Fig. 6f–h, the tensile strength, Young's modulus, and tensile strain at break of pure PVA film are about 23.30 MPa, 33.86 MPa, and 383.28%, respectively, indicating a typical soft and toughness characteristic. After introducing HNFs obtained from bamboo into PVA matrix (with a 2% TEMPO-B loading), the tensile

strength, Young's modulus, and tensile strain at break are 42.63 MPa, 853.42 MPa, and 242.19%, respectively. In terms of composite film with 2% MNF-B, the tensile strength, Young's modulus, and tensile strain at break are 40.09 MPa, 810.24 MPa, and 235.29%, respectively. Compared with pure PVA film, the tensile strength and modulus remarkably increased while elongation at break decreased, indicating that the composite films changed from soft and tough to rigid and tough. In particular, the Young's modulus of HNFs/PVA is 25.12 times higher than that of pure PVA. The increase in the tensile strength and Young's modulus upon HNF loading is mainly due to that the PVA and HNF surface contains plentiful hydroxyl functional groups, and the hydrogen bonding network can be formed during the film-forming process. This result can be verified by previous work (Okahisa et al. 2020; Qua et al. 2009).

Conclusions

In summary, a series of novel holocellulose nanofibers of different plants (wheat straw, bamboo, hardwood, and softwood) were obtained through sodium hypochlorite/acetic acid delignification, followed by defibrillation using an ultrafine pulverizer. HNFs prepared by mechanical method exhibit high hemicellulose content, well preserved natural structure (cellulose is coated with hemicellulose, the hemicellulose is considered as a polymer matrix phase), and high crystallinity. As a contrast, the natural structure of holocellulose nanofiber prepared by TEMPO-mediated oxidation method was destroyed, the content of hemicellulose and the crystallinity are dramatically decreased. After introducing HNFs into PVA matrix, the mechanical properties of HNFs/PVA composite films are dramatically enhanced. Especially, the Young's modulus of HNFs/PVA composite film is 25.12 times higher than that of pure PVA. The presented results suggest that holocellulose nanofiber can be used as versatile reinforcement to replace nanocellulose to construct composite materials with high performance.

Acknowledgments This work was supported by the Beijing Forestry University Outstanding Young Talent Cultivation Project (2019JQ03017), Beijing Municipal Natural Science Foundation (6222044), and Ministry of Education, China-111 Project (BP0820033).

Funding The authors have not disclosed any funding.

Declarations

Conflict of interest All the authors declare that there are no conflicts of interest.

References

Abdul Khalil HPS, Davoudpour Y, Islam MN, Mustapha A, Sudesh K, Dungani R, Jawaid M (2014) Production and modification of nanofibrillated cellulose using various mechanical processes: a review. Carbohydr Polym 99:649–665. https://doi.org/10.1016/j.carbpol.2013.08.069

Alila S, Boufi S, Belgacem MN, Beneventi D (2005) Adsorption of a cationic surfactant onto cellulosic fibers I. Surface charge effects. Langmuir 21(18):8106–8113. https://doi.org/10.1021/la050367n

Altman R (2021) The myth of historical bio-based plastics. Science 373(6550):47–49. https://doi.org/10.1126/science.abj1003

Alves L, Ferraz E, Lourenço AF, Ferreira PJ, Rasteiro MG, Gamelas JAF (2020) Tuning rheology and aggregation behaviour of TEMPO-oxidised cellulose nanofibrils aqueous suspensions by addition of different acids. Carbohydr Polym 237:116109. https://doi.org/10.1016/j.carbpol.2020.116109

Arola S, Malho JM, Laaksonen P, Lille M, Linder MB (2013) The role of hemicellulose in nanofibrillated cellulose networks. Soft Matter 9(4):1319–1326. https://doi.org/10.1039/C2SM26932E

Bahsi Kaya G, Kim Y, Callahan K, Kundu S (2022) Microencapsulated phase change material via pickering emulsion stabilized by cellulose nanofibrils for thermal energy storage. Carbohydr Polym 276:118745. https://doi.org/10.1016/j.carbpol.2021.118745

Chaker A, Alila S, Mutjé P, Vilar MR, Boufi S (2013) Key role of the hemicellulose content and the cell morphology on the nanofibrillation effectiveness of cellulose pulps. Cellulose 20(6):2863–2875. https://doi.org/10.1007/s10570-013-0036-y

Chen L, Zhu JY, Baez C, Kitin P, Elder T (2016) Highly thermal-stable and functional cellulose nanocrystals and nanofibrils produced using fully recyclable organic acids. Green Chem 18(13):3835–3843. https://doi.org/10.1039/C6GC00687F

Chen Y, Geng B, Ru J, Tong C, Liu H, Chen J (2017) Comparative characteristics of TEMPO-oxidized cellulose nanofibers and resulting nanopapers from bamboo, softwood, and hardwood pulps. Cellulose 24(11):4831–4844. https://doi.org/10.1007/s10570-017-1478-4

Ferrer A, Filpponen I, Rodríguez A, Laine J, Rojas OJ (2012) Valorization of residual empty palm fruit bunch fibers (EPFBF) by microfluidization: Production of nanofibrillated cellulose and epfbf nanopaper. Bioresource

Technol 125:249–255. https://doi.org/10.1016/j.biortech.2012.08.108
Fukuzumi H, Saito T, Okita Y, Isogai A (2010) Thermal stabilization of TEMPO-oxidized cellulose. Polym Degrad Stabil 95(9):1502–1508. https://doi.org/10.1016/j.polymdegradstab.2010.06.015
Galland S, Berthold F, Prakobna K, Berglund LA (2015) Holocellulose nanofibers of high molar mass and small diameter for high-strength nanopaper. Biomacromolecules 16(8):2427–2435. https://doi.org/10.1021/acs.biomac.5b00678
Gao Y, Lipton AS, Wittmer Y, Murray DT, Mortimer JC (2020) A grass-specific cellulose–xylan interaction dominates in sorghum secondary cell walls. Nat Commun 11(1):6081. https://doi.org/10.1038/s41467-020-19837-z
Habibi Y, Lucia LA, Rojas OJ (2010) Cellulose nanocrystals: Chemistry, self-assembly, and applications. Chem Rev 110(6):3479–3500. https://doi.org/10.1021/cr900339w
Hausmann MK, Siqueira G, Libanori R, Kokkinis D, Neels A, Zimmermann T, Studart AR (2020) Complex-shaped cellulose composites made by wet densification of 3D printed scaffolds. Adv Funct Mater 30(4):1904127. https://doi.org/10.1002/adfm.201904127
Isobe N, Chen X, Kim UJ, Kimura S, Wada M, Saito T, Isogai A (2013) TEMPO-oxidized cellulose hydrogel as a high-capacity and reusable heavy metal ion adsorbent. J Hazard Mater 260:195–201. https://doi.org/10.1016/j.jhazmat.2013.05.024
Isogai A, Saito T, Fukuzumi H (2011) TEMPO-oxidized cellulose nanofibers. Nanoscale 3(1):71–85. https://doi.org/10.1039/C0NR00583E
Jia C, Chen C, Mi R, Li T, Dai J, Yang Z, Pei Y, He S, Bian H, Jang S-H, Zhu JY, Yang B, Hu L (2019) Clear wood toward high-performance building materials. ACS Nano 13(9):9993–10001. https://doi.org/10.1021/acsnano.9b00089
Jiang F, Hsieh Y-L (2013) Chemically and mechanically isolated nanocellulose and their self-assembled structures. Carbohydr Polym 95(1):32–40. https://doi.org/10.1016/j.carbpol.2013.02.022
Kang X, Sun P, Kuga S, Wang C, Zhao Y, Wu M, Huang Y (2017) Thin cellulose nanofiber from corncob cellulose and its performance in transparent nanopaper. ACS Sustain Chem Eng 5(3):2529–2534. https://doi.org/10.1021/acssuschemeng.6b02867
Khawas P, Deka SC (2016) Isolation and characterization of cellulose nanofibers from culinary banana peel using high-intensity ultrasonication combined with chemical treatment. Carbohydr Polym 137:608–616. https://doi.org/10.1016/j.carbpol.2015.11.020
Kim HJ, Roy S, Rhim JW (2021) Effects of various types of cellulose nanofibers on the physical properties of the CNF-based films. J Environ Chem Eng 9(5):106043. https://doi.org/10.1016/j.jece.2021.106043
Klemm D, Heublein B, Fink H-P, Bohn A (2005) Cellulose: Fascinating biopolymer and sustainable raw material. Angew Chem Int Edit 44(22):3358–3393. https://doi.org/10.1002/anie.200460587
Kontturi E, Tammelin T, Österberg M (2006) Cellulose-model films and the fundamental approach. Chem Soc Rev 35(12):1287–1304. https://doi.org/10.1039/B601872F
Li T, Zhai Y, He S, Gan W, Wei Z, Heidarinejad M, Dalgo D, Mi R, Zhao X, Song J, Dai J, Chen C, Aili A, Vellore A, Martini A, Yang R, Srebric J, Yin X, Hu L (2019) A radiative cooling structural material. Science 364(6442):760–763. https://doi.org/10.1126/science.aau9101
Liu P, Guo X, Nan F, Duan Y, Zhang J (2017) Modifying mechanical, optical properties and thermal processability of iridescent cellulose nanocrystal films using ionic liquid. ACS Appl Mater Inter 9(3):3085–3092. https://doi.org/10.1021/acsami.6b12953
Liu X, Jiang Y, Song X, Qin C, Wang S, Li K (2019) A biomechanical process for cellulose nanofiber production-towards a greener and energy conservation solution. Carbohydr Polym 208:191–199. https://doi.org/10.1016/j.carbpol.2018.12.071
Liu P, Pang B, Dechert S, Zhang XC, Andreas LB, Fischer S, Meyer F, Zhang K (2020) Structure selectivity of alkaline periodate oxidation on lignocellulose for facile isolation of cellulose nanocrystals. Angew Chem Int Edit 59(8):3218–3225. https://doi.org/10.1002/anie.201912053
Liu W, Du H, Liu K, Liu H, Xie H, Si C, Pang B, Zhang X (2021) Sustainable preparation of cellulose nanofibrils via choline chloride-citric acid deep eutectic solvent pretreatment combined with high-pressure homogenization. Carbohydr Polym 267:118220. https://doi.org/10.1016/j.carbpol.2021.118220
MacLeod M, Arp HPH, Tekman MB, Jahnke A (2021) The global threat from plastic pollution. Science 373(6550):61–65. https://doi.org/10.1126/science.abg5433
Nakagaito AN, Yano H (2004) The effect of morphological changes from pulp fiber towards nano-scale fibrillated cellulose on the mechanical properties of high-strength plant fiber based composites. Appl Phys A 78(4):547–552. https://doi.org/10.1007/s00339-003-2453-5
Nascimento ES, Pereira ALS, Barros MdO, Barroso MKdA, Lima HLS, Borges MdF, Feitosa JPdA, de Azeredo HMC, Rosa MdF (2019) TEMPO oxidation and high-speed blending as a combined approach to disassemble bacterial cellulose. Cellulose 26(4):2291–2302. https://doi.org/10.1007/s10570-018-2208-2
Niu X, Liu Y, Fang G, Huang C, Rojas OJ, Pan H (2018) Highly transparent, strong, and flexible films with modified cellulose nanofiber bearing UV shielding property. Biomacromolecules 19(12):4565–4575. https://doi.org/10.1021/acs.biomac.8b01252
Okahisa Y, Matsuoka K, Yamada K, Wataoka I (2020) Comparison of polyvinyl alcohol films reinforced with cellulose nanofibers derived from oil palm by impregnating and casting methods. Carbohydr Polym 250:116907. https://doi.org/10.1016/j.carbpol.2020.116907
Oksanen T, Buchert J, Viikari L (1997) The role of hemicelluloses in the hornification of bleached kraft pulps. Holzforschung 51(4):355–360. https://doi.org/10.1515/hfsg.1997.51.4.355
Peng F, Ren JL, Xu F, Bian J, Peng P, Sun RC (2009) Comparative study of hemicelluloses obtained by graded ethanol precipitation from sugarcane bagasse. J Agr Food Chem 57(14):6305–6317. https://doi.org/10.1021/jf900986b

Peng F, Bian J, Peng P, Xiao H, Ren JL, Xu F, Sun RC (2012) Separation and characterization of acetyl and non-acetyl hemicelluloses of arundo donax by ammonium sulfate precipitation. J Agr Food Chem 60(16):4039–4047. https://doi.org/10.1021/jf3000828

Qua EH, Hornsby PR, Sharma HSS, Lyons G, McCall RD (2009) Preparation and characterization of poly(vinyl alcohol) nanocomposites made from cellulose nanofibers. J Appl Polym Sci 113(4):2238–2247. https://doi.org/10.1002/app.30116

Rao J, Lv Z, Ding Q, Chen G, Hao X, Bian J, Guan Y, Peng F (2021) Rapid processing of holocellulose-based nanopaper toward an electrode material. ACS Sustain Chem Eng 9(8):3337–3346. https://doi.org/10.1021/acssuschemeng.0c09408

Saito T, Yanagisawa M, Isogai A (2005) TEMPO-mediated oxidation of native cellulose: SEC–malls analysis of water-soluble and -insoluble fractions in the oxidized products. Cellulose 12(3):305–315. https://doi.org/10.1007/s10570-004-5835-8

Saito T, Kimura S, Nishiyama Y, Isogai A (2007) Cellulose nanofibers prepared by TEMPO-mediated oxidation of native cellulose. Biomacromolecules 8(8):2485–2491. https://doi.org/10.1021/bm0703970

Santos RG, Machovsky-Capuska GE, Andrades R (2021) Plastic ingestion as an evolutionary trap: Toward a holistic understanding. Science 373(6550):56–60. https://doi.org/10.1126/science.abh0945

Simmons TJ, Mortimer JC, Bernardinelli OD, Pöppler AC, Brown SP, deAzevedo ER, Dupree R, Dupree P (2016) Folding of xylan onto cellulose fibrils in plant cell walls revealed by solid-state NMR. Nat Commun 7(1):13902. https://doi.org/10.1038/ncomms13902

Sluiter A, Hames B, Ruiz R, Scarlata C, Sluiter J, Templeton D, Crocker D (2008) Determination of structural carbohydrates and lignin in biomass. Lab Anal procedure 1617:1–16

Timell T (1967) Recent progress in the chemistry of wood hemicelluloses. Wood Sci Technol 1(1):45–70. https://doi.org/10.1007/BF00592255

Van Hai L, Zhai L, Kim HC, Kim JW, Choi ES, Kim J (2018) Cellulose nanofibers isolated by TEMPO-oxidation and aqueous counter collision methods. Carbohydr Polym 191:65–70. https://doi.org/10.1016/j.carbpol.2018.03.008

Wang S, Cheng Q (2009) A novel process to isolate fibrils from cellulose fibers by high-intensity ultrasonication, part 1: Process optimization. J Appl Polym Sci 113(2):1270–1275. https://doi.org/10.1002/app.30072

Wang QQ, Zhu JY, Gleisner R, Kuster TA, Baxa U, McNeil SE (2012) Morphological development of cellulose fibrils of a bleached eucalyptus pulp by mechanical fibrillation. Cellulose 19(5):1631–1643. https://doi.org/10.1007/s10570-012-9745-x

Wang Y, Zhang L, Liu W, Cui C, Hou Q (2019) Fabrication of optically transparent and strong nanopaper from cellulose nanofibril based on corncob residues. Carbohydr Polym 214:159–166. https://doi.org/10.1016/j.carbpol.2019.03.035

Wang M, Yu T, Tan L, Li W, Wei W, Jiang M, Liu D, Zhou Z (2020) An eco-friendly approach to preparing cellulose nanocrystals by precisely controlling the dissolution of natural cellulose in TBAH/H_2O solvent. Cellulose 27(16):9311–9324. https://doi.org/10.1007/s10570-020-03418-w

Wang Z, Lee YH, Kim SW, Seo JY, Lee SY, Nyholm L (2021) Why cellulose-based electrochemical energy storage devices? Adv Mater 33(28):2000892. https://doi.org/10.1002/adma.202000892

Wei J, Jia S, Wei J, Ma C, Shao Z (2021) Tough and multifunctional composite film actuators based on cellulose nanofibers toward smart wearables. ACS Appl Mater Inter 13(32):38700–38711. https://doi.org/10.1021/acsami.1c09653

Yang H, Yan R, Chen H, Lee DH, Zheng C (2007) Characteristics of hemicellulose, cellulose and lignin pyrolysis. Fuel 86(12):1781–1788. https://doi.org/10.1016/j.fuel.2006.12.013

Yang X, Berthold F, Berglund LA (2019) High-density molded cellulose fibers and transparent biocomposites based on oriented holocellulose. ACS Appl Mater Inter 11(10):10310–10319. https://doi.org/10.1021/acsami.8b22134

Yang X, Reid MS, Olsén P, Berglund LA (2020) Eco-friendly cellulose nanofibrils designed by nature: Effects from preserving native state. ACS Nano 14(1):724–735. https://doi.org/10.1021/acsnano.9b07659

Zhang L, Tsuzuki T, Wang X (2015) Preparation of cellulose nanofiber from softwood pulp by ball milling. Cellulose 22(3):1729–1741. https://doi.org/10.1007/s10570-015-0582-6

Zhao Y, Moser C, Lindström ME, Henriksson G, Li J (2017) Cellulose nanofibers from softwood, hardwood, and tunicate: Preparation–structure–film performance interrelation. ACS Appl Mater Inter 9:13508–13519. https://doi.org/10.1021/acsami.7b01738

Zhu H, Luo W, Ciesielski PN, Fang Z, Zhu JY, Henriksson G, Himmel ME, Hu L (2016) Wood-derived materials for green electronics, biological devices, and energy applications. Chem Rev 116(16):9305–9374. https://doi.org/10.1021/acs.chemrev.6b00225

Zhu C, Liu P, Mathew AP (2017) Self-assembled TEMPO cellulose nanofibers: Graphene oxide-based biohybrids for water purification. ACS Appl Mater Inter 9(15):21048–21058. https://doi.org/10.1021/acsami.7b06358